Packing arrangement of the three cone classes in primate retina

Austin Roorda [a],*, Andrew B. Metha [b], Peter Lennie [c], David R. Williams [d]

[a] *University of Houston College of Optometry, Houston, TX 77204-6052, USA*
[b] *Department of Optometry and Vision Sciences, The University of Melbourne, Melbourne, Australia*
[c] *Center for Neural Science, New York University, New York, NY, USA*
[d] *University of Rochester, Center for Visual Science, Rochester, NY, USA*

Abstract

We describe a detailed analysis of the spatial arrangement of L, M and S cones in the living eyes of two humans and one monkey. We analyze the cone mosaics near 1° eccentricity using statistical methods that characterize the arrangement of each type of cone in the mosaic of photoreceptors. In all eyes, the M and L cones are arranged randomly. This gives rise to patches containing cones of a single type. In human, but not in monkey, the arrangement of S-cones cannot be distinguished from random. © 2001 Elsevier Science Ltd. All rights reserved.

Keywords: Photoreceptors; Cones; Retina; Imaging; Mosaic

1. Introduction

Spatial vision and color vision depend on the same mosaic of cone photoreceptors, yet their demands are different and to some extent in conflict. Fine spatial vision is best served if photoreceptors all have the same spectral sensitivity, so that local variations in the signals originating in different cones represent only differences in intensity and not differences in spectral composition. On the other hand, to resolve fine variations in the spectral composition of a scene requires neighboring photoreceptors to have different spectral sensitivities. The visual system must therefore inevitably compromise in balancing good spatial vision against good color vision.

In the trichromatic eyes of humans and old-world primates, the spatial structure of images is conveyed predominantly via the middle (M) and long (L) wavelength sensitive cones (Lennie, Pokorny, & Smith, 1993), which have similar spectral sensitivities, and whose signals will be highly correlated when confronted with stimuli of the same spectral composition. The spectral sensitivity of the short wavelength sensitive (S)

cones is shifted well toward shorter wavelengths, so within the whole mosaic of cones there will be substantial variations in local signal arising from differences in spectral sensitivity rather than local variations in intensity. S cones are relatively sparse in human (absent in the central fovea) and monkey retinas and comprise usually < 10% of the total cone population (Curcio, Allen, Sloan, Lerea, Hurley, Block, & Milam, 1991). This low density mitigates the chromatic contamination of spatial vision, and is sufficient to capture the coarse image structure typically available at short wavelengths as a result of chromatic aberration. To obtain a more complete understanding of the tradeoff between spatial vision and color vision, we need to know how L and M cones are distributed on the retina.

S cones are readily identified histochemically (Curcio et al., 1991; de Monasterio, McCrane, Newlander, & Schein, 1985) and by a subtly distinctive morphology (Ahnelt, Kolb, & Pflug, 1987) but no similarly straightforward methods exist for distinguishing between L and M cones and discovering their distributions. Several investigators have attempted to distinguish the L and M cones in primates, and to map their mosaics. Marc and Sperling (1977) identified S, M and L cones by their reaction to nitroblue tetrazolium chloride (NBT) when preferentially excited with different wavelengths of light. L, M and S cones were identified in one of

---

* Corresponding author. Tel.: +1-713-7431952; fax: +1-713-7432053.

E-mail address: aroorda@uh.edu (A. Roorda).

three retinal samples. Marc and Sperling found that the L:M ratio was $\sim 0.6{:}1$ and that L cones were arranged randomly. Mollon and Bowmaker (1992) used axial microspectrophotometry to measure the spectra of individual cones in the retina of the talapoin monkey. In five separate patches containing altogether 183 cones they found a L:M ratio of 0.93:1 and concluded that the arrangement of L and M cones was locally random. Calkins, Schein, Tsukamoto, and Sterling (1994), using electron microscopic images of macaque retina, identified two non-S-cone classes of cones by virtue of a sharply bimodal distribution of the number of synaptic contacts individual cones made with bipolar cells. These two cone types (in a sample of 108 cones near the foveola) were distributed randomly. Calkins et al. suggested that the two classes might be M and L cones. Packer, Williams, and Bensinger (1996) used axial densitometry to identify cones in patches of excised macaque retina. On one sample of peripheral retina they measured a ratio of 1.17:1 and concluded that the L and M cones were slightly clumped.

In the human eye, Gowdy and Cicerone (1998) attempted to identify individual L and M cones in the fovea using a psychophysical method. The interpretation of results hinges on several assumptions, one of which is that stable fixation better than 2 min of arc can be maintained for > 7000 psychophysical trials. They reported a random arrangement of cones for two subjects (subject 1, 49 cones, L:M = 1.45:1; subject 2, 31 cones, L:M = 1.21:1). A study at 17° eccentricity by the same group found a random arrangement of L and M cones (subject 1, 71 cones, L:M = 1.7:1; subject 2, 72 cones, L:M = 1.9:1) (Otake, Gowdy, & Cicerone, 2000). More recently, Roorda and Williams measured the arrangement of M and L cones in living human eyes using spatially localized retinal densitometry made possible by adaptive optics (Roorda & Williams, 1999), and concluded that the L and M cones were randomly arranged in the mosaic.

Here, we present a fuller analysis of the S, M and L cone mosaics in the human retina and add to it an analysis of the arrangement of cones in a macaque retina (Roorda, Metha, Lennie, & Williams, 1999). We find in both species the distribution of M and L cones is random. The distribution of S cones appears to be random in the human retina but not in the monkey.

2. Methods

2.1. Adaptive optics retinal imaging

We used the Rochester Adaptive Optics Ophthalmoscope (developed in David Williams' laboratory) to resolve single photoreceptors in the living eye. Full details of the imaging technique, and its application in

imaging the cones in human retina are described in Liang, Williams, and Miller (1997). In short, the aberrations of the eye, which normally impose a limit on what features can be resolved on the retina, are corrected using adaptive optics. After compensation for aberrations in this manner, the lateral resolution of retinal images is increased about three times over conventional imaging methods, allowing virtually all cone photoreceptors to be seen in retinal images.

2.1.1. Animal and human selection, preparation and imaging

Retinal imaging experiments were attempted on a total of seven monkey eyes, before the start of physiological recordings made as part of other experiments. Each monkey was anesthetized initially with ketamine hydrochloride (Vetalar, 10 mg/kg, i.m.). Cannulae were inserted in the saphenous veins, and the trachea was cannulated. Surgery was continued under sufentanil citrate (Sufenta) anesthesia. The head was placed in a stereotaxic frame mechanically coupled to the optical system with a rigid six-axis goniometer mount, whose center of rotation was about the pupil center. By adjusting the goniometer we could select the retinal location at which measurements were made. Guided by experience gained during the course of imaging the human retina, we chose a location 1° from the ophthalmoscopically identified fovea, just outside the foveal avascular zone. Electrodes were attached to the head to monitor the electroencephalogram (EEG), and to the forearms to monitor electrocardiogram (ECG). No procedure (other than the initial injection) was undertaken without anesthesia.

After surgery, anesthesia was maintained by a continuous infusion of Sufenta (initially 4 mg/kg/h) in a solution of lactated Ringer's solution and dextrose. The adequacy of this dose was ensured by observing the monkey for 3 h before administering muscle relaxant. The dose was increased if the animal showed any signs of arousal. After the observation period, a loading dose of vecuronium bromide (Norcuron) was infused rapidly to induce paralysis, which was maintained by a continuous infusion of Norcuron (100 mg/kg/h). The monkey was ventilated at 20 strokes/min at a tidal volume adjusted to keep the end-tidal CO_2 close to 33 mm Hg. The EEG and ECG were monitored continuously, and at any sign of arousal the anesthetic dose was increased. A heating blanket controlled by a subscapular thermistor kept the animal's body temperature near 37°C.

Pupils were dilated with atropine sulfate and the corneas were protected with rigid gas permeable contact lenses, which had been stored in soaking solution. These remained in place for the duration of the measurements (Metha, Crane, Rylander, Thomsen & Albrecht, 2000). Metal speculae kept the eyelids retracted while a series of 1° circular images were successively

acquired under fully bleached, dark adapted and selectively bleached conditions over the course of ∼ 16 h. During some, but not all initial experiments, we noticed that it became progressively more difficult to obtain high-contrast retinal images beyond several hours. This appeared not to result from a change in optical aberrations caused by physical deformation of the eye over time, for it could not be corrected by the adaptive optical system. Rather, because we found that image quality could be restored by wetting and cleaning the anterior surface of the contact lens in situ, we suspect that the anterior lens surface was acting as an increasing source of scatter over this time period. Increasing the ambient humidity and changing the contact lens material (from Fluroperm 92 to Boston ES) appeared to improve the situation for later experiments.

The eyes of the two human subjects were dilated with 1% cyclopentolate prior to imaging. To maintain stability and optical alignment, the subjects bit into a dental impression mount that was affixed to an X–Y–Z translation stage. Both humans had normal color vision. One subject, AN, was selected for the imaging study after ERG measurements indicated that he had a low L:M cone ratio (Brainard et al., 2000). More details on the imaging methods and results can be found in our earlier publications (Roorda & Williams, 1999; Williams & Roorda, 2000).

All experiments on human subjects were done with their understanding and informed written consent. The experiments on both human and monkeys were carried out in accordance with written guidelines by the NIH and were approved by the University of Rochester Institutional Review Board.

2.2. Spatially resolved retinal densitometry

To identify specific cone subtypes we combined retinal densitometry (Campbell & Rushton, 1955; Rushton & Baker, 1964) with high-resolution imaging (Roorda & Williams, 1999). Small (1° circular) patches of the retina located ∼ 1° from the fovea were photographed using a 4 ms flash of 550 nm light, a wavelength chosen to maximize the absorptance by L and M cone photopigments. Individual cones were classified by comparing images taken when the photopigment was fully bleached with those taken when it was either dark-adapted or exposed to a light that selectively bleached one photopigment. Images of fully bleached retina were obtained following exposure to 550 nm light (70 nm bandwidth, 37×10^6 td s). Images of dark-adapted retina were taken following 5 min spent in darkness. From these images, we created absorptance images, defined as 1 minus the ratio of a dark adapted or selectively bleached image and the corresponding fully bleached image. The ratio is calculated for each corresponding pixel in the two registered images.

The first step in distinguishing S from M and L cones was to generate absorptance images between dark adapted and fully bleached images in the manner described above. Since the S cones absorb negligibly while the M and L cones absorb strongly at the imaging wavelength of 550 nm, the S cones appear as a sparse array of dark cones in the absorptance image while the M and L cones appear bright. Variations in absolute pigment absorptance due to, for example, systematic changes in outer segment length, prevented us from identifying all of the S cones using a single absorptance criterion across the entire patch of retina. A subset of cones that did not meet the criterion but were suspected S-cones because their absorptance was substantially lower than that of other cones in the neighborhood were also selected as S. Once this sparse population was identified, these cones were removed from the analysis to facilitate the identification of the M and L cones.

To distinguish L and M cones, we took images immediately following each of two bleaching conditions. In the first condition, the dark-adapted retina was exposed to a 650 nm light that selectively bleached the L pigment. In the second condition, the dark-adapted retina was exposed to a 470 nm light that selectively bleached the M pigment. The absorptance image for the 650 nm bleach revealed dark, low absorptance L cones that had been heavily bleached and bright, highly-absorbing M cones spared from bleaching. The absorptance images for the 470 nm bleach showed the opposite arrangement.

Bleaching levels had to be carefully set to maximize the difference in photopigment concentration between the L and M cone classes, since over-bleaching at any wavelength would leave too little pigment in either type of cone to be useful for identification purposes. Using the wavelength of the bleaching light, and our best knowledge of the spectral absorptances of the L and M cones (Baylor, Nunn, & Schnapf, 1987), we calculated their respective bleaching rates. Then we calculated at what bleaching level the maximum difference in concentration would occur, and the total concentration of the pigment at that point. Given this concentration, we calculated what the expected reflectance of a contiguous mosaic of cones in the retina should be, relative to the dark-adapted and fully bleached reflectance. We set the optimal bleaching levels empirically, by regulating the bleach energy until we obtained the desired retinal reflectance, relative to the fully bleached and dark-adapted retinal reflectance. One caveat is that, to calculate the desired reflectance, one needs to know the relative proportions of the L and M cones, which was initially unknown. We initially assumed an L:M ratio of 2:1 and as the experiment progressed we altered the bleaching energy to reflect the actual L:M ratio.

To avoid bleaching the pigment we were trying to measure, we used as little light as possible. As a result,

the photon noise in the images was high, and the signal-to-noise ratio low. To improve signal-to-noise to a level that made it possible to identify cones reliably, between 20 and 40 images were taken for each bleaching condition. These were later registered by maximizing the cross-correlation between pairs of images and were then added together.

The final steps in identifying L and M cones were to plot the relative absorptance of each cone after a 650 nm bleach against its absorptance after a 470 nm bleach (Fig. 1(A), inset). L cones preferentially absorb long wavelength light, and so have low absorptance after a 650 nm bleach. On the other hand, after a 470 nm bleach, L cone absorptance is relatively high. Thus, in Fig. 1(A) (inset), L cones are represented by the lower right collection of data points while M cones cluster in the top left. There is much variation in these data, a significant source of which appears to come from the differences in the absorptance of light by individual cones, i.e. some cones absorb a lot of light after bleaching by both 470 and 650 nm light, while other cones do not absorb much at all, thus spreading data points to greater or lesser extent radially out from the zero-absorptance origin. These differences are likely due to differences in photopigment concentration of each cone. In any case, the variance that arises from a range of absorptances systematically radiates from the origin.

Therefore, by considering only the polar angle (θ) of each data point, we can concern ourselves with the remaining source of variation in the data, which is due to differences in selective absorption of L and M cones:

$$\theta = \frac{\text{Absorptance after 650nm bleach}}{\text{Absorptance after 470nm bleach}}$$

Cones were identified as L or M by fitting a sum of two Gaussian distributions to the histogram and designating cones on left and right side of the intersection as L or M cones respectively. We can estimate how many cones are misidentified by calculating the fraction of each distribution that falls on the wrong side of the dividing criterion.

2.3. Analysis of cone arrangement

All analyses were done using programs written in Matlab. The cone datasets are available for downloading from: http://www.opt.uh.edu/research/aroorda/ao_res.htm.

We examined whether or not the three different cone types were distributed randomly, whether there was any tendency for S cones to contact either L or M cones preferentially and whether there was a tendency for S-cones to reside at discontinuities in the close-packed mosaic.
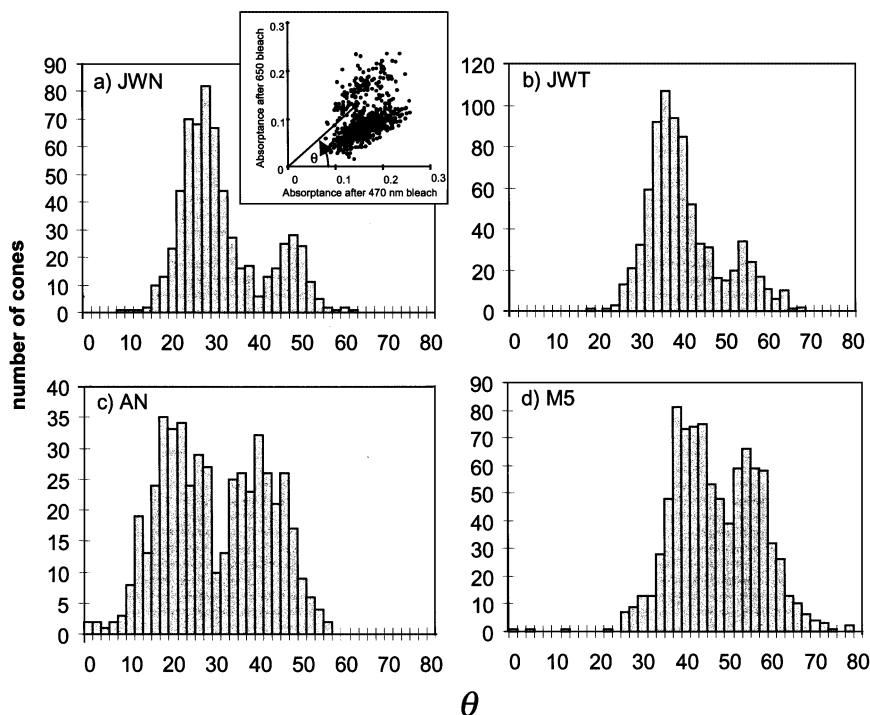

Fig. 1. The inset shows, for each cone, the absorptance following a 650 nm bleach vs. the absorptance of the same cone following a 470 nm bleach. Since L-cones are more preferentially bleached by the 650 nm light, it is expected that they will occupy the lower distribution along the 650 nm bleaching axis. To analyze further, we calculate histograms of the number of cones as a function of angle on the plot where the angle is shown in the figure. The histograms show a bimodal distribution. Cones were identified as L or M by fitting a sum of two Gaussians to the histogram and designating cones on either side of the intersection as L or M. S-cones are not included in these histograms.

a) JWN　　　　　　　　　　　　　　　**b) JWT**

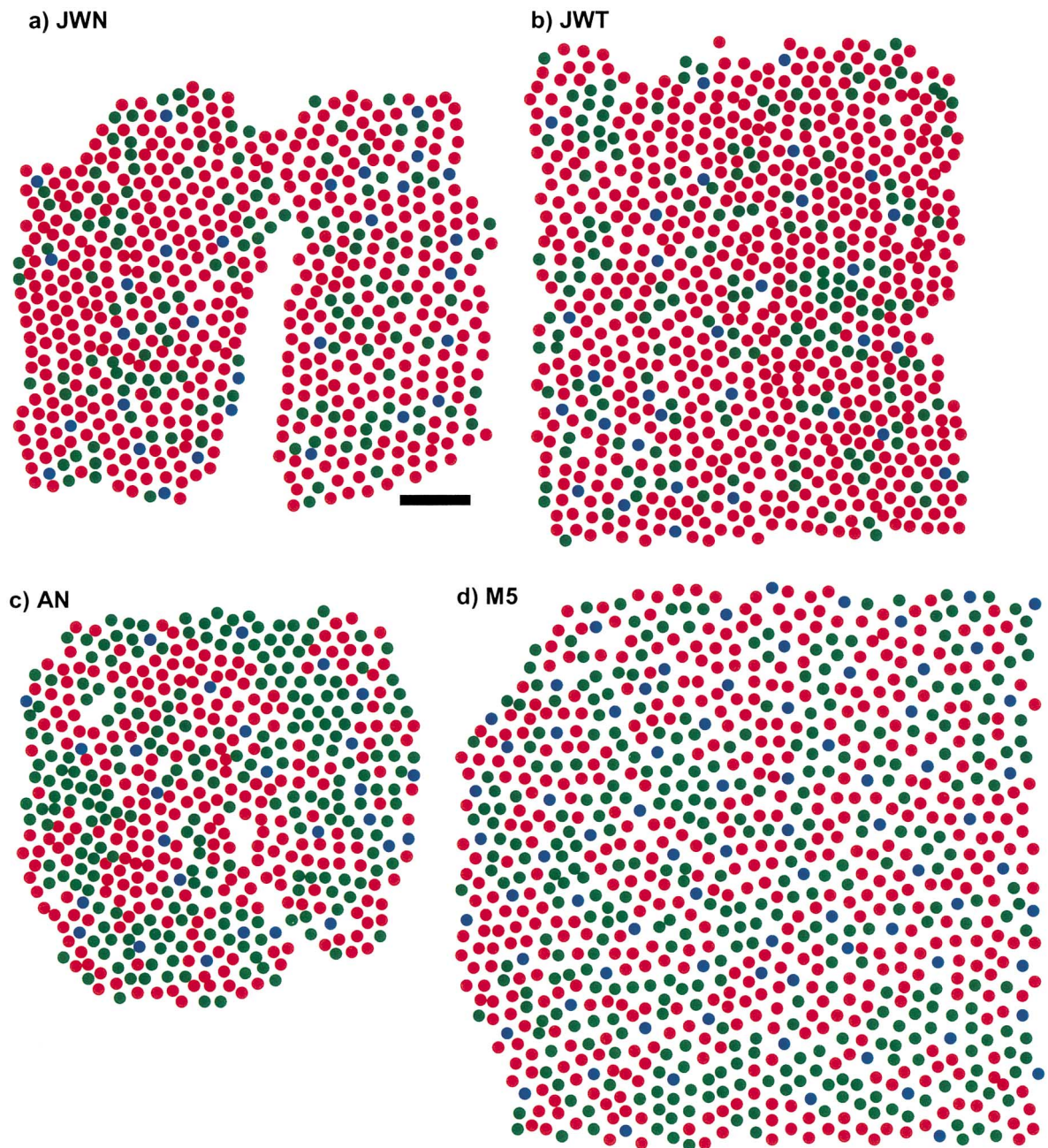**c) AN**　　　　　　　　　　　　　　　**d) M5**

Fig. 2. L, M and S cone mosaics for two humans: JW (a nasal and a temporal location is shown, labeled JWN and JWT, respectively); and AN, and one macaque, M5. L, M and S cones are shown as red, green and blue dots respectively. For JWN, a patch of central cones was not identified due to a capillary that obscured those cones. All mosaics are shown to the same scale. Scale bar = 5 μm.

To determine whether or not the arrangement of the different classes of cones is random we extract an appropriate arrangement-dependent statistic from the real mosaic, and from simulations in which the same mosaic of cone locations is populated randomly by L, M and S cones in their observed proportions. This process is referred to as a Monte Carlo simulation. Since our simulations use the known cone locations from the original dataset, the statistics we extract are sensitive only to differences in cone identity and not to differences in cone location.

Two methods were adopted to establish whether the different classes of cones were randomly distributed or more systematically placed within the mosaic. The first method was developed by Rodieck (1991). A second method, which we include in Appendix A, is from Diggle (1983). These methods use different approaches but both provide a statistic that characterizes the degree of randomness in cone arrangement. If the statistic calculated from the real mosaic falls within the bounds of the distribution of the statistic calculated from the multiple simulations, we deem the arrangement of the

Table 1
Summary of cone numbers, ratios and estimated errors for four datasets[a]

Dataset	Location imaged	# of cones	# L	# M	# S	L:M ratio	L:M assignment error (%)	S cone%
JWN	1° nasal	650	487	133	30	3.66:1	1	4.6
JWT	1° temporal	811	621	159	31	3.9:1	3	3.8
AN	1° nasal	522	264	231	27	1.14:1	5.6	5.2
M5	1.4° nasal	904	482	344	78	1.40:1	6	8.6
M3	∼1° nasal	507	–	–	39	–	–	7.7
M6	∼1° nasal	625	–	–	41	–	–	6.6
M7	∼1° nasal	583	–	–	37	–	–	6.3

[a] Three monkeys had S-cones analyzed only. All four monkeys were male.

Table 2
Summary of S-cone proportions from the present study and from the literature

Author	Species (number)	S-cone proportion	Retinal location	Method
Present study	Human (2)	4.5%	1°	Retinal densitometry
Bumstead and Hendrickson (1999)	Human (4)	8%	∼0.75°	Immunocytochemistry
Curcio et al. (1991)	Human (6)	4%	1°	Immunocytochemistry
Ahnelt et al. (1987)	Human (3)	15%	1°	Morphology
Present study	Macaque (4)	7.3%	1–1.5°	Retinal densitometry
de Monasterio et al. (1985)	Macaque (1)	13%	1°	Intracellular staining
Bumstead and Hendrickson (1999)	Macaque (2)	25%	∼1°	Immunocytochemistry
Marc and Sperling (1977)	Baboon (1)	20%	1°	Staining
Mollon and Bowmaker (1992)	Talapoin (?)	3%	Fovea	Microspectrophotometry

different classes of cones in the real mosaic to be random. Both methods yield the same results.

2.3.1. The density recovery profile

Rodieck (1991) described a technique for measuring whether or not a mosaic is randomly distributed. If the arrangement of a particular class of cones in an array were random, the spatial density of those cones (represented by points) would be the same in any given annulus surrounding a particular cone, regardless of the radius of the annulus. If cones of a particular type segregate themselves, then the density of cones of that type will be lowest in the immediate vicinity of each of them. On the other hand, if there is a propensity for clumping, the density of cones will be higher in the immediate vicinity of each of them. The plot of average cone density vs. radial distance from the cone is called the density recovery profile (DRP) and can be shown as a histogram. This histogram is uniform when the cones are randomly distributed.

To establish whether or not cones in real mosaics were randomly distributed, we generated DRPs for 100 synthetic mosaics in which the observed number of L and M cones were distributed randomly, and for each DRP calculated the root mean square (RMS) of the difference between it and the average of all simulations. We also calculated the rms difference between the DRP of the real mosaic and average of all simulations. For the real mosaic to be considered non-random it had to

meet two conditions: the rms error had to rank above the 95th percentile ($P < 0.05$) in the distribution of errors for synthetic random mosaics, and each bin in the histogram for the real mosaic had to lie within two standard deviations ($P < 0.046$) of the range of cone densities for each bin in the average histogram. This is a very restrictive condition when one considers that the simulations themselves are generated by a random process.

2.3.2. Corrections for misidentified cones

Optical blur reduces contrast in the image and makes cone types less distinguishable, because some of the light attributed to any individual cone in the image actually derives from the cones surrounding it. The probability of misidentifying a cone depends on the

Table 3
Test of whether S-cones prefer to neighbor either L or M cones[a]

Dataset	Fraction of surrounding M/L × 100	Expected fraction % ± 1 SD
JWN	22.7273	21.4516 ± 3.09416
JWT	22.1649	20.3846 ± 2.89234
AN	47.561	46.6667 ± 3.89566
M5	40	41.6465 ± 2.41991

[a] The observed fraction of cones surrounding the S-cones is no different than is expected from a random distribution of M and L cones. S-cones have no tendency to neighbor either L or M cones.

Table 4
Average number and standard deviation of cones within a 1.5 arcmin circle (1.75 arcmin for macaques) surrounding L, M and S cones[a]

Dataset	L-cones	M-cones	S-cones
JWN	6.37 ± 0.70 (n = 395)	6.49 ± 0.81 (n = 109)	6.16 ± 0.80 (n = 25)
JWT	6.64 ± 0.81 (n = 528)	6.61 ± 0.90 (n = 141)	6.41 ± 0.63 (n = 29)[b]
AN	6.57 ± 0.89 (n = 231)	6.47 ± 0.79 (n = 190)	6.19 ± 0.87 (n = 21)
M5	6.81 ± 0.80 (n = 413)	6.85 ± 0.82 (n = 311)	6.69 ± 0.68 (n = 62)[b]
	L or M cones		S-cones
M3	6.26 ± 0.74 (n = 391)		6.30 ± 0.68 (n = 33)
M6	6.14 ± 0.75 (n = 493)		5.92 ± 0.77 (n = 36)
M7	8.43 ± 1.16 (n = 448)		8.40 ± 1.25 (n = 30)

[a] In all cases, there is no large difference in the number nor in the standard deviation of cones surrounding either L, M or S cones.
[b] Values which do not lie within the 95% range according to the F-test.

types of cones surrounding it. For example, if an M cone is surrounded by L cones, it will appear more like an L cone. When such a cone is misidentified, one might incorrectly interpret the mosaic as being more clumped than it is. Even when the error is as small as it is in our datasets, this potential clumping artifact can have serious results.

To deal with the potential blurring artifact, we examined the effect of changing the identity of cones that were in clumps and most likely misidentified. We did this by picking cones that were: (1) surrounded by more than two-thirds of the same cone type; and (2) were the least confidently identified by densitometry (i.e. cones that were closest to the overlap of the two Gaussian distributions of cones in Fig. 1). When a mosaic appeared to be more clumped than would be expected from random assignment of cones, we changed the assigned identities of individual cones that best met the selection criteria, noting how many changes were necessary to render the mosaic random.
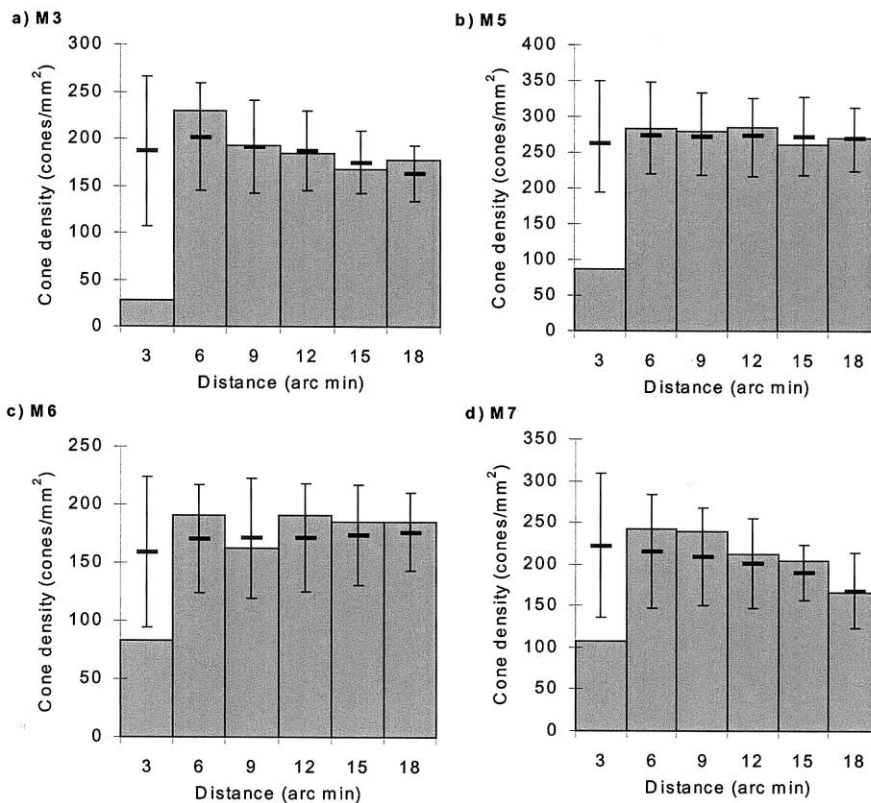
Fig. 3. Density recovery profiles (DRPs) of the S cones for four macaque eyes. The cone density is averaged in annular rings of 3 arcmin radius, out to 18 arcmin. Experimental DRPs are represented by the solid bars. Dashes with error bars represent the average ± 2 SD of the 100 random simulations. The mosaic for each macaque shows a low density in the vicinity of the central cone, implying that the array is more regularly spaced, or more crystalline, than a random array.
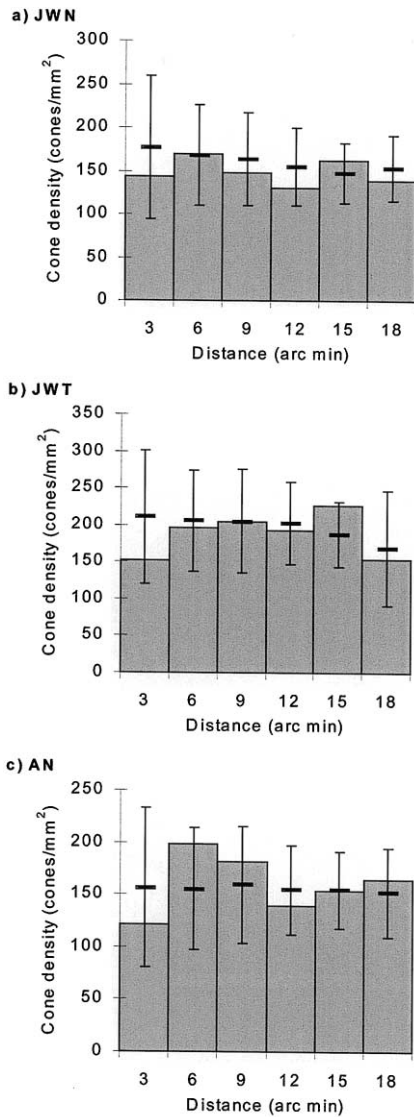
Fig. 4. Density recovery profiles (DRPs) of the S cones for two human eyes. The cone density is averaged in annular rings of 3 arcmin radius, out to 18 arcmin. Experimental DRPs are represented by the solid bars. Dashes with error bars represent the average plus and minus 2 SD of the 100 random simulations. The S-cone mosaics for JWN, JWT and AN are no different from random.

3. Results

Fig. 2 shows the L, M and S cone mosaics for two locations in one human eye, one location in a second human eye and in one macaque eye. Cone numbers and estimated errors in the identification of L and M cones are listed in Table 1. The S-cones, but not the L and M cones, could be identified in three other macaques and their details are included in Table 1.

3.1. S-cones

The proportions of S cones we found in human and macaque lay near the low ends of the ranges measured using other techniques. Table 2 summarizes prior and current results.

3.1.1. Nearest neighbors

We first examined whether S-cones might show a tendency to neighbor either L or M cones in the retina. To examine this idea we measured the ratio of M to L cones in a zone of radius 1.5 min (1.75 min of arc for M5) surrounding each S cone and compared this with values expected from the simulations. The zone size was chosen so that only the nearest neighbors would be counted. The expected ratio of M/L cone contacts and its standard deviation were computed from the overall ratio of M−L cones and the total number of observations made. The results in Table 3 show that the ratio of M and L cones surrounding S cones is the same as the overall ratio of M and L cones in the mosaic. We conclude that there is no tendency for S-cones to associate preferentially with L or M cones.

It has been suggested that S cones tend to lie at discontinuities in an otherwise close-packed (hexagonal) cone mosaic (Ahnelt et al., 1987; Pum, Ahnelt, & Grasl, 1990). A cone at a discontinuity in a hexagonally packed mosaic would be surrounded by either 5 or 7 nearest neighbors, rather than the usual 6. To test this hypothesis, we counted the average number and standard deviation of the number of cones surrounding each cone (Table 4). If the S cones tended to lie at discontinuities, then the standard deviation of the number of cones surrounding them would be higher than for M and L cones. Two datasets showed a significant difference (*F*-test, $P < 0.05$) in the standard deviation between the S-cones and the L or M cones. In our case, however, the S-cones showed less variation and thus were in the opposite direction. In both cases, the differences were marginal and we found no evidence to support Ahnelt et al's hypothesis. It should be added here that our analysis is on living, functioning tissue and is not subject to any histological artifact.

3.1.2. Density recovery profile

Fig. 3 (humans) and Fig. 4 (macaques) show density recovery profiles for the S-cones in the real mosaic (filled bars) and the simulations (horizontal line ± 2 SD). For the three human datasets, the density at all radial distances lay within two standard deviations of the random simulations, so we conclude that S cones are distributed randomly. The DRPs for the macaque retinas show fewer short intercone distances than would be found in a random mosaic, indicating that the S-cones tend to segregate themselves.
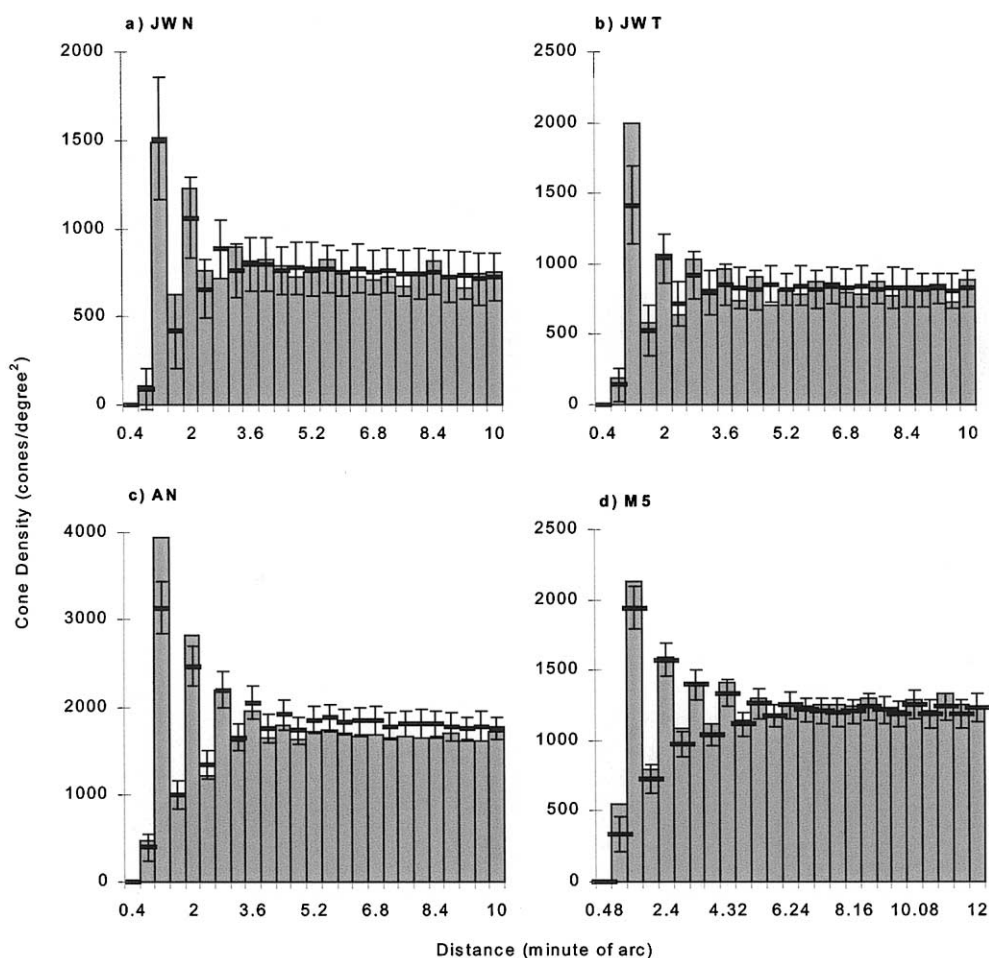
Fig. 5. DRPs of the M cones for each dataset. The cone density is averaged in annular rings of 0.4 min of arc out to 10 min. The solid bars represent the DRP of the experimental mosaic. The dashes with errors bars represent the average ± 2 SD of the 100 random simulations. Cone densities oscillate in the nearest annular rings because of the nearly triangular packing structure in the mosaic. The first peak represents the ring of nearest neighbors in the close-packed mosaic. JWN is the only mosaic for which all experimental density values lie within the limits of the simulations.

3.2. L and M cones

The proportions of L and M cones in the four datasets are listed in Table 1. These are quite different in the two human retinas. For two reasons this seems not to reflect local variations across the retina, but rather a genuine difference between individuals. First, subject JW showed no significant difference in the ratio at 1° nasal and 1° temporal. Second, ERG measurements on the same individuals over a 59° field yielded similar differences in the ratio (Brainard et al., 2000).

3.2.1. Density recovery profiles

Fig. 5 shows DRPs for the M cone distributions in the four original mosaics. DRPs for both the experimental data and simulations show a series of oscillatory peaks and troughs in density for annuli of small diame-

Table 5
Ranking of experimental DRP (between the experimental DRP and the average simulated DRP) with 100 random rms deviations (between each simulated DRP and the average simulated DRP)[a]

Dataset	# of cones swapped for DRP	Rank of DRP test (out of 100 trials)
JWN	0	67
JWT	0	100[b,c]
JWT adjusted	16	87
AN	0	100[b,c]
An adjusted	32	90
M5	0	99[b,c]
M5 adjusted	36	76

[a] The second column shows the number of cones that had to be switched to render the mosaic random according to the Rodieck test.
[b] Significantly different from random according to rank score.
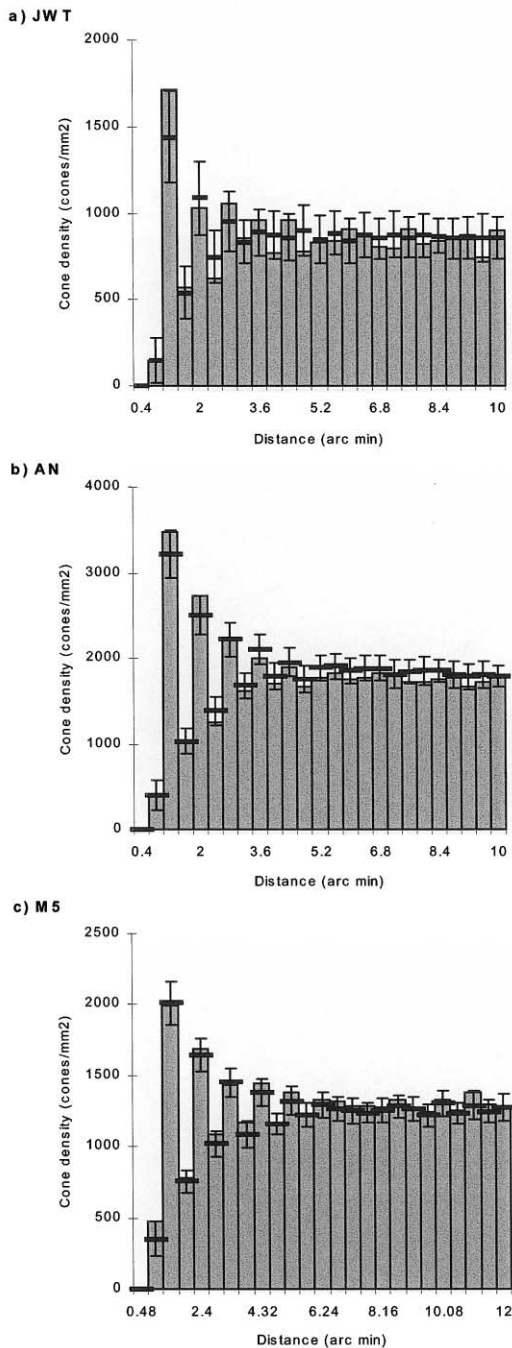[c] Some points lie outside of the upper and lower limits of the 100 random simulations.

Fig. 6. DRPs of the adjusted M-cone arrays for JWT, AN, and M5. After adjusting the assignment of cones in the mosaic to correct for possible errors due to optical blur, all mosaics became indistinguishable from random.

RMS error ranking of the other three cases were all greater than 95 out of 100, signifying a cone arrangement pattern different to that expected from random assignment ($P < 0.05$). Inspection of these DRPs reveal that over short distances, the experimentally measured density is significantly greater than the density expected from random assignment, indicating slight clumping of the M-cones.
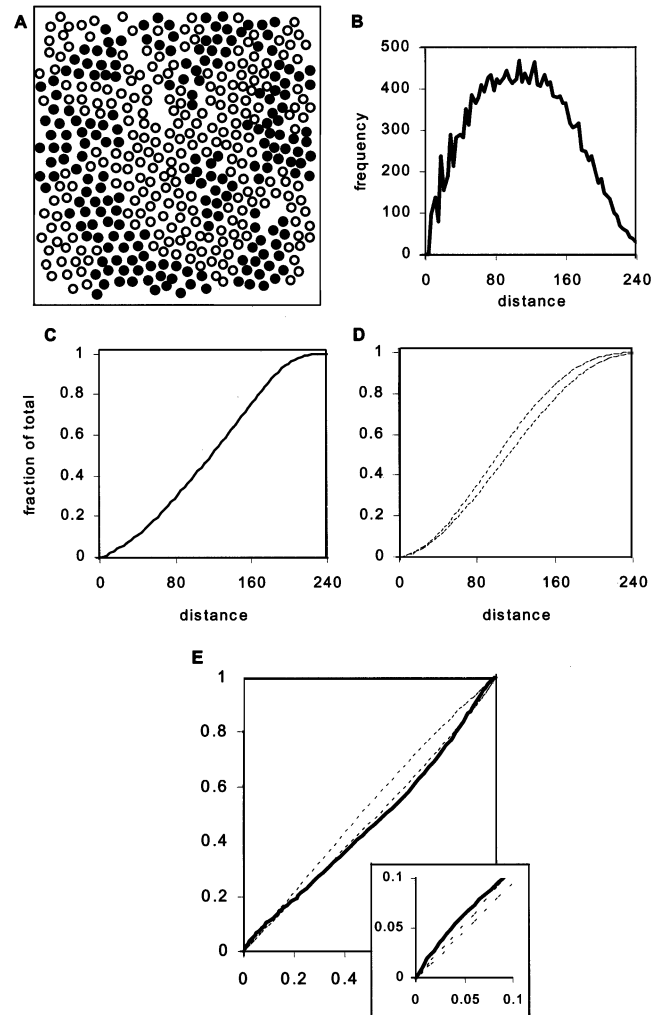

Fig. A1. Computation of spatial distribution of cones. (a) Locations of all the cones in the dataset. The mosaic shown here is a set of actual cone locations (AN) with, for this simulation, the cone types arbitrarily assigned. The cone distribution that will be analyzed is represented by the solid circles. Random simulations are generated by assigning fixed numbers of L, M and S cones randomly to locations within the same mosaic. (b) Histogram of all the intercone distances measured for the solid black circles in (a). The total number of distances for *n* cones is $n*(n-1)$. (c) Cumulative (integrated) histogram of (b) (d) The thin lines represent the maximum and minimum values of the cumulative histograms for 100 simulations, each comprised of the same number of cones. (e) Solid line: Cumulative histogram comparison (CHC) plot, which is the average cumulative histogram of (d) versus the cumulative histogram of (c). Dashed lines: minimum and maximum of 100 cumulative histograms versus cumulative histogram in (d). The inset shows that the simulated mosaic of (a) is clumped (non-random) on a local scale.

ter. This is an expected pattern of results given the interaction of a continuously expanding cone-centered analysis ring and the close-packed nature of cones in our images. Moreover, it affects equally the results derived from real and simulated mosaics, and is therefore not relevant to our analysis. The DRPs show that only one mosaic, JWN, satisfies our dual condition for complete spatial randomness. Table 5 shows that the
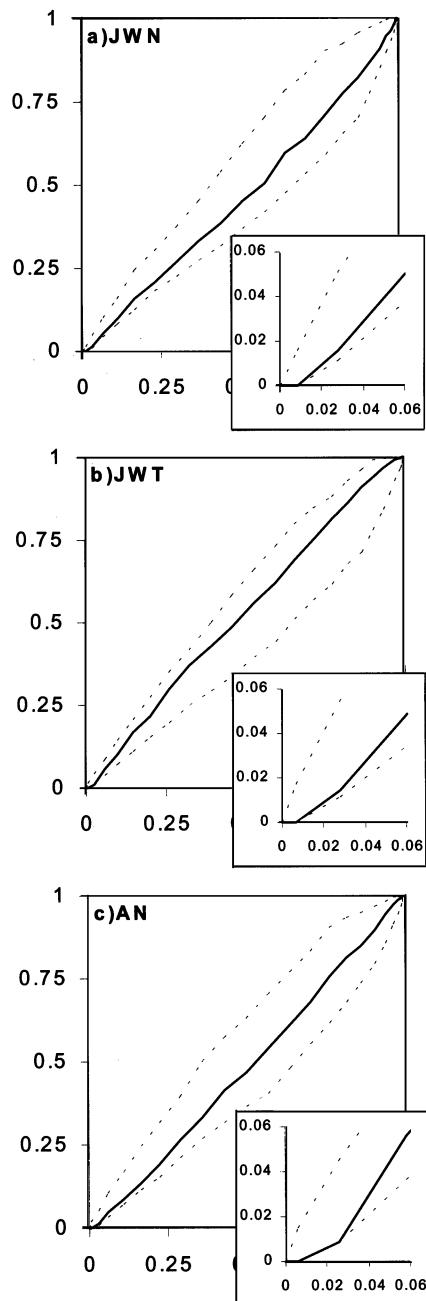
Fig. A2. Cumulative histogram comparisons (CHCs) for the S cones for the two human subjects. The graph shows the fraction of the total number of cones with increasing distance from any cone, for the random simulations and the experimental dataset, respectively. Dashed lines represent the upper and lower bounds of the 100 random simulations. The inset shows a magnified view of the lower left corner of the CHC graph. If the experimental line lies outside the upper or lower bound of the random simulations, then the mosaic is deemed different from random. Both human have S cone arrangements at this location that are not significantly different from random.

To test whether misidentification of cones might have given rise to spurious clumping, we changed the identities of those cones that were most susceptible to being misidentified (see Section 2). We did this cone-by-cone until the mosaic became indistinguishable from random. For JWT, 16 cones (2% of L and M cones) required their identities changed. For AN, 32 cones (6.1% of L and M cones) were changed, and for M5 36 (4% of L and M cones) cones were changed. The results are listed in Table 5. The number of cones changed was very close to the number expected to be misidentified (Table 1). Even after these adjustments, the (now random) mosaics maintained their rather patchy appearance. DRPs for the adjusted mosaics are shown on Fig. 6. The analysis of the L cone mosaics showed that in all cases they had the same properties as M cone mosaics.

4. Discussion

4.1. Comparison with other studies

Our finding that the S-cones near the fovea in the human eye are arranged randomly agrees with Curcio et al. (1991). We also agree with Curcio et al. (1991) and others (Ahnelt et al., 1987; Shapiro, Schein, & de Monasterio, 1985) that the macaque retina, which generally lacks a tritanopic zone (Bumstead & Hendrickson, 1999; Ahnelt et al., 1987), has S-cones at locations near 1° eccentricity that are more regularly distributed.

The randomness in the L and M cone mosaics agree with other studies (Mollon & Bowmaker, 1992; Calkins et al., 1994; Marc & Sperling, 1977; Gowdy & Cicerone, 1998).

4.2. Apparent aggregation and optical blur

Optical blur provides a simple explanation of the apparent aggregation of M-cones in all three of our datasets that initially appeared non-random. Moreover, the fraction of cones whose identities had to be changed to make each mosaic random was correlated with the estimated error in cone assignment. Assignment errors were also correlated with subjective estimates of optical blur in the images. It is not surprising then, that the mosaic with the smallest assignment error, JWN at 1%, was deemed random according to all tests.

Progenitor cells in the developing retina may 'bias' their progeny to express either M or L pigment, leading one to expect a clumpy mosaic. The lack of clumping might reflect the extensive migration of cones that is known to occur near the fovea during development (Packer, Hendrickson, & Curcio, 1990). Cones might be genuinely clumped in peripheral retina, where there is less migration (Packer et al., 1990).

4.3. Consequences of random mosaics for vision

The fact that the three cone classes are constrained to a two-dimensional surface means that on a spatial scale

of the size of a single cone, the eye cannot distinguish colors. The patchiness of the mosaic that results from random arrangement of cones only serves to increase the size of these color-blind spots. Even after correction for misidentified cones, all four mosaics analyzed here had patches, 5 arcmin or more across, that contained only one of the two longer wavelength-sensitive types. The presence of these color-blind patches should lead to oddities of color appearance in spatial patterns of finer granularity than the patches. This seems to happen. In the illusion known as Brewster's colors, irregular splotches of pastel color are seen while viewing periodic, back and white patterns of high spatial frequency (Brewster, 1832). Similarly, red-green isoluminant gratings with spatial frequencies above the resolution limit look like chromatic and luminance spatial noise (Sekiguchi, Williams, & Brainard, 1993). These perceptual errors are examples of the aliasing that is produced when the three cone submosaics sample the retinal image inadequately. The errors are analogous to the chromatic errors that can be seen in images taken with digital cameras that have interleaved pixels of different spectral sensitivity (Williams,

Sekiguchi, Haake, Brainard, & Packer, 1991). The patchiness that results from the aggregation of M and L cones reported here will exacerbate the effects of aliasing.

Patches of cones of a single type will be disadvantageous when the image contains chromatic modulation of high spatial frequency, though in normal life its adverse effects will be diminished by chromatic aberration (Marimont & Wandell, 1992). Furthermore, even though patchiness implies that the trichromat will sometimes misjudge the color appearance of tiny objects, it can benefit the perception of high frequency luminance patterns because cortical neurons tuned to high spatial frequencies are more likely to be fed by contiguous cones of the same class. For low spatial frequencies (to which the chromatic system is most sensitive) clumping could be advantageous, for it would facilitate the assembly of spatially coarse sampling mechanisms that drew their inputs from a single class of cone. Hsu, Smith, Buchsbaum, and Sterling (2000) have suggested that electrical coupling among cones could provide some beneficial pooling of signals, though signals could equally well be summed later.
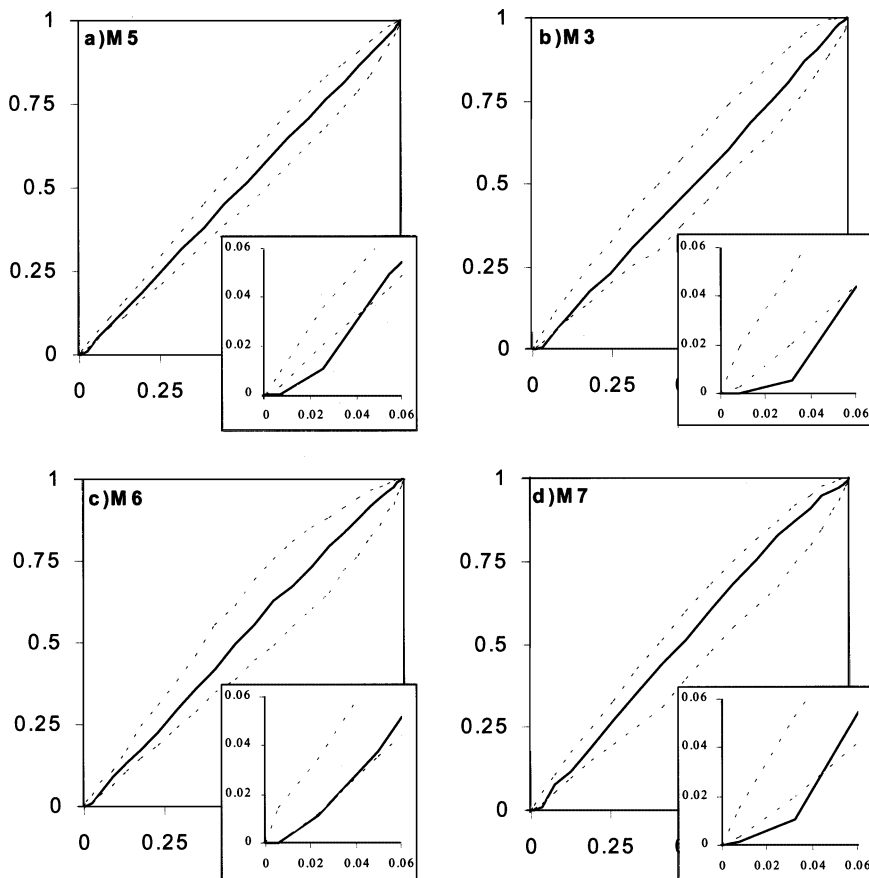

Fig. A3. Cumulative histogram comparisons (CHCs) for the S cones for four macaques. Every macaque retina shows an S cones arrangement that is more regular than random.
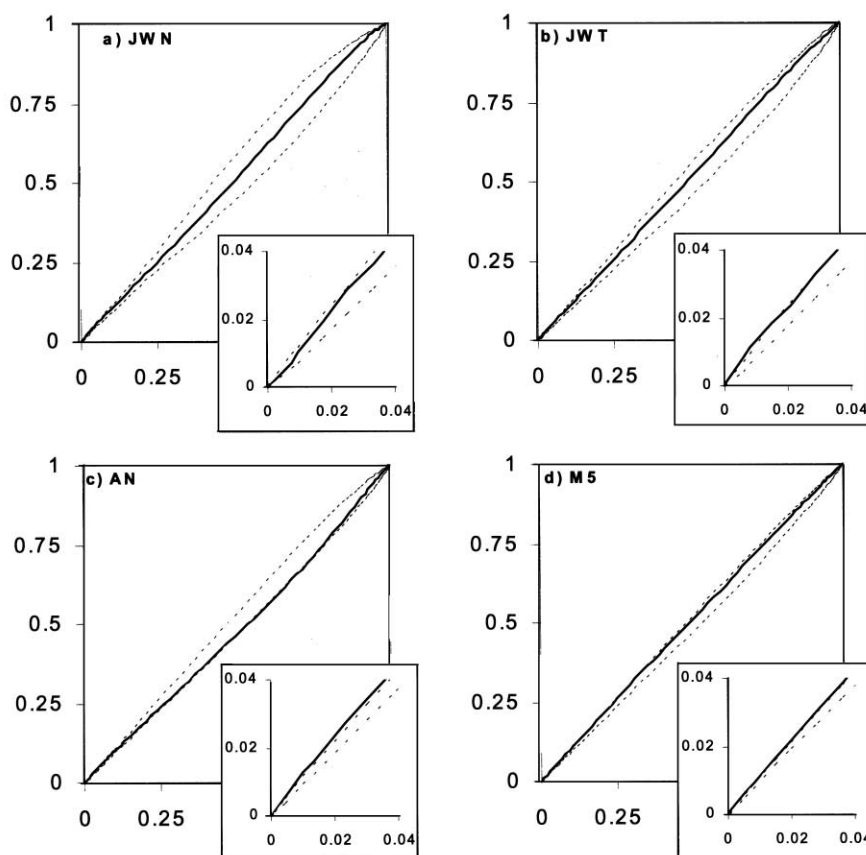
Fig. A4. CHCs of the M-cone array for the four datasets. JWN is the only mosaic for which all points in the experimentally derived cumulative histogram lie within the upper and lower bounds of the random simulations. Close inspection (see insets to each figure) shows that the mosaics for JWT, AN, and M5 are slightly more clumped than a random array.

4.4. Implications of random mosaics for retinal wiring

How the patchy mosaic that results from random assignments affects the organization of color-opponent pathways will depend on whether the L-M color opponent mechanism makes principled or random connections with L and M cones. Midget ganglion cells provide the only known pathway for carrying the L–M color-opponent signal out of the retina. These ganglion cells have color-opponent receptive fields, in which centers and surrounds have different spectral sensitivities. Within several degrees of the fovea each midget ganglion cell receives its input from a single midget bipolar cell; in peripheral retina it is driven by several bipolar cells (Dacey, 1999). Each midget bipolar cell receives signals directly from a single cone that forms the center of its receptive field, and it probably derives its surround from the H1 horizontal cell (Dacey, Diller, Verweij, & Williams, 2000a). The surround of the ganglion cell's receptive field probably arises in the surrounds of the bipolar cells that drive it (Dacey et al., 2000b).

In or near the fovea, a midget ganglion cell will receive direct input (forming the center of its receptive field) almost exclusively from a single cone. Any effects of cone clumping will be expressed through the receptive field surround. The best available evidence, both anatomical (Goodchild, Chan, & Grünert, 1996) and physiological (Dacey, 1996) suggests that the surround is formed by indiscriminate drawing on all neighboring L and M cones, rather than by principled selection of one type of cone. Patches of cones of a single type will therefore give rise to surround signals whose spectral weighting, in different cells, could vary from all M to all L. One might therefore expect the degree of color opponency to vary among ganglion cells, and this has been found (Derrington, Krauskopf, & Lennie, 1984). The fact that the centers and surrounds of midget ganglion cells are well-balanced in strength will to some extent mitigate the effects of variations in L and M cone input to the surround (Lennie, Haake, & Williams, 1991).

In peripheral retina, receptive fields of midget ganglion cells no longer have centers driven by a single cone. The available evidence (Dacey, 1996) suggests that centers do not select for a single class of cone, so color opponency in the periphery will be weakened to the extent that both center and surround receive signals

from both L and M cones. When ganglion cells draw their inputs indiscriminately from both L and M cones, patches of cones of one type then become potentially beneficial, for they increase the probability that the centers of at least some ganglion cell receptive fields are driven by cones of a single class.
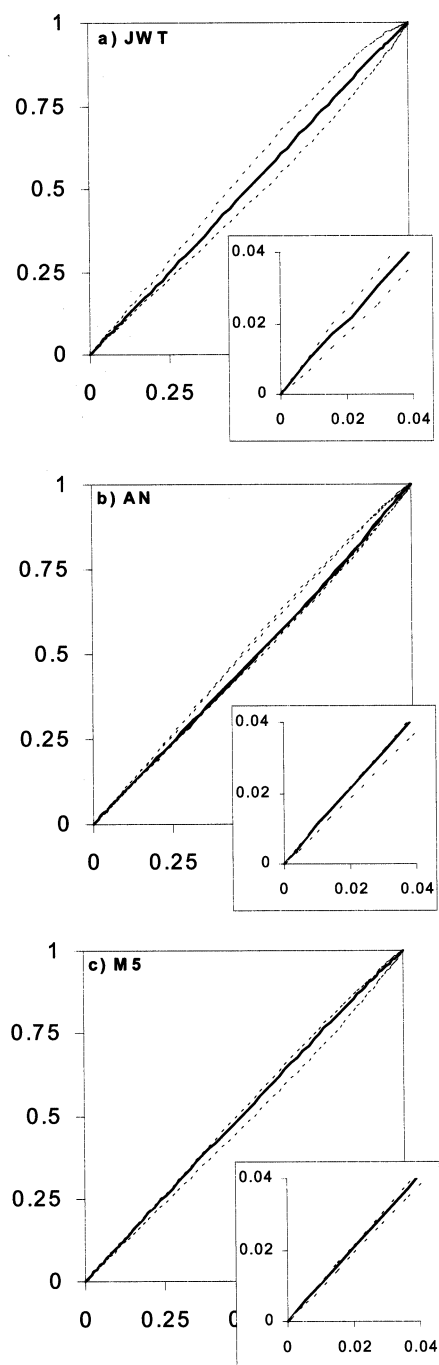

Fig. A5. CHCs' of the adjusted M-cone array for JWT, AN, and M5. After adjusting the mosaic for possible errors due to optical blur, all mosaics became indistinguishable from random.

4.5. Monte Carlo simulation

We used Monte Carlo simulations to test whether or not the arrangements of S, M and L cones could be random. Each simulation used the same set of cone locations to which the constant numbers of S, M and L cones were randomly assigned. The great benefit of the Monte Carlo approach was that it obviated the need to develop a larger theoretical model that accounted for the locations of cones in the mosaic. This in turn made it easy to apply two rather stringent tests for random arrangement of cones.

5. Conclusions

The arrangement of S, M and L cones near the fovea in the human can be considered to be random. Given the size of our sample, randomness represents a very narrow and restrictive condition among the range of possible mosaics that can be formed. Therefore, we conclude that the apparently small tendency toward aggregation in some of the datasets is likely an artifact of the small amount of optical blur in the images. The arrangement in the macaque retina is similar to humans except that S cones lie in a more crystalline mosaic.

Appendix A

A.1. Method

Using Diggle's analysis (Diggle, 1983), we measured all the intercone distances between the cones of a single type (L, M or S) within the array. Then we generated a histogram of the frequency of occurrence of all intercone distances for a single cone-type as a function of distance. The histogram was integrated and normalized to one, and was called the cumulative histogram. The cumulative histogram represents the fraction of the total number of cones that falls within a specified radius. A cumulative histogram is used because it is a monotonically increasing function and lends itself to a comparison with the random simulations. The comparison of two cumulative histograms is called a cumulative histogram comparison, or CHC. If the two histograms are identical, the CHC yields a 1:1 line. The stages in the analysis are shown in Fig. A1. Several statistics were drawn from the analysis. First, we computed the root mean square (RMS) deviation of the experimental curve from the average of all the random samples. We then ranked the RMS of the experimental mosaic among a set of the same statistic computed for each of the random simulations. If the rank was 95th percentile or higher, the experimental data set was deemed different from random by that scale ($P < 0.05$). If, at any

distance, the value of the dataset exceeded the range of the 100 simulated mosaics, then the mosaic was also deemed to be non-random ($P < 0.01$).

A.2. S-cones

The cumulative histogram comparison plots for the two humans and the four macaques are shown on Figs. A2 and A3. These plots show that the S-cone distributions are no different from random for the three human datasets. The macaque shows a departure from randomness. Closer inspection of the CHC plot for M5 (Fig. A2(d) inset) shows that there are too few short intercone distances. This indicates that the S-cones for the macaque retina tend to segregate themselves and approach a crystalline arrangement.

A.3. L and M cones

The CHC plots for our measured cone mosaics are shown in Fig. A4. Only one mosaic, JWN, is truly random according to the strict conditions we applied. In the other three cases, there was slight clumping of the M-cones at short distances, shown by the experimental statistic lying above the upper bound of the range of all 100 random simulations (see the enlarged inset for each plot). The mosaics were deemed random after a small correction for possible misidentified cones that resides in clump in the mosaic (see Section 2). The CHC plots for the adjusted mosaics are shown on Fig. A5. The number of cone changes required to return the array to random is listed in Table A1, and in all cases were close the number of assignment changes that were required to render mosaics random according the DRP-based statistics listed in Table 5.

References

Ahnelt, P. K., Kolb, H., & Pflug, R. (1987). Identification of a subtype of cone photoreceptor, likely to be blue sensitive, in the human retina. *Journal of Comparative Neurology*, 255, 18–34.

Baylor, D. A., Nunn, B. J., & Schnapf, J. L. (1987). Spectral sensitivity of cones of the monkey *Macaca Fascicularis*. *Journal of Physiology*, 390, 145–160.

Brainard, D. H., Roorda, A., Yamauchi, Y., Calderone, J. B., Metha, A. B., Neitz, M., Neitz, J., Williams, D. R., & Jacobs, G. H. (2000). Functional consequences of individual variation in relative L and M cone numerosity. *Journal of the Optical Society of America A*, 17, 607–614.

Brewster, D. (1832). On the undulations excited in the retina by the action of luminous points and lines. *London Edinburgh Philosophical Magazine Journal of Science*, 1, 169–174.

Bumstead, K., & Hendrickson, A. (1999). Distribution and development of short-wavelength cones differ between macaca monkey and human fovea. *Journal of Comparative Neurology*, 403, 502–516.

Calkins, D. J., Schein, S. J., Tsukamoto, Y., & Sterling, P. (1994). M and L cones in macaque fovea connect to midget ganglion cells by different numbers of excitatory synapses. *Nature*, 371, 70–72.

Campbell, F. W., & Rushton, W. A. H. (1955). Measurement of the scotopic pigment in the living human eye. *Journal of Physiology*, 130, 131–147.

Curcio, C. A., Allen, K. A., Sloan, K. R., Lerea, C. L., Hurley, J. B., Block, I. B., & Milam, A. H. (1991). Distribution and morphology of human cone photoreceptors stained with anti-blue opsin. *Journal of Comparative Neurology*, 312, 610–624.

Dacey, D. (1999). Primate retina: cell types, circuits and color opponency. *Progress in Retinal and Eye Research*, 18, 737–763.

Dacey, D. M. (1996). Circuitry for color coding in the primate retina. *Proceedings of the National Academy of Science USA*, 93, 582–588.

Dacey, D. M., Diller, L. C., Verweij, J., & Williams, D. R. (2000a). Physiology of L- and M-cone inputs to H1 horizontal cells in the primate retina. *Journal of the Optical Society of America A*, 17, 589–596.

Dacey, D. M., Packer, O. S., Diller, L., Brainard, D., Peterson, B., & Lee, B. (2000b). Center surround receptive field structure of cone bipolar cells in primate retina. *Vision Research*, 40, 1801–1811.

de Monasterio, F. M., McCrane, E. P., Newlander, J. K., & Schein, S. J. (1985). Density profile of blue-sensitive cones along the horizontal meridian of macaque retina. *Investigative Ophthalmology and Visual Science*, 26, 289–302.

Derrington, A. M., Krauskopf, J., & Lennie, P. (1984). Chromatic mechanisms in lateral geniculate nucleus of macaque. *Journal of Physiology (London)*, 357, 241–265.

Diggle, P.J. (1983). Statistical Analysis of Spatial Point Patterns, London: Academic Press.

Goodchild, A. K., Chan, T. L., & Grünert, U. (1996). Horizontal cell connections with short wavelength sensitive cones in macaque monkey retina. *Visual Neuroscience*, 13, 833–845.

Gowdy, P. D., & Cicerone, C. M. (1998). The spatial arrangement of the L and M cones in the central fovea of the living human eye. *Vision Research*, 38, 2575–2589.

Hsu, A., Smith, R., Buchsbaum, G., & Sterling, P. (2000). Cost of cone coupling to trichromacy in primate fovea. *Journal of the Optical Society of America A*, 17, 635–640.

Lennie, P., Haake, W., & Williams, D.R. (1991). The design of chromatically opponent receptive fields. In: Landy, M.S. & Movshon, J.A. (Eds.), Computational Models of Visual Processing. Cambridge, MA: MIT Press, pp. 71–82.

Lennie, P., Pokorny, J., & Smith, V. C. (1993). Luminance. *Journal of the Optical Society of America A*, 10, 1283–1293.

Liang, J., Williams, D. R., & Miller, D. (1997). Supernormal vision and high-resolution retinal imaging through adaptive optics. *Journal of the Optical Society of America A*, 14, 2884–2892.

Marc, R. E., & Sperling, H. G. (1977). Chromatic organization of primate cones. *Science*, 196, 454–456.

Marimont, D. H., & Wandell, B. A. (1992). Linear models of surface and illuminant spectra. *Journal of the Optical Society of America A*, 9, 1905–1913.

Metha, A.B., Crane, A.M., Rylander III, H.G., Thomsen, S.L., & Albrecht, D.G. (2000). Maintaining the cornea and general physiological environment in visual neurophysiology experiments, in preparation

Mollon, J. D., & Bowmaker, J. K. (1992). The spatial arrangement of cones in the primate fovea. *Nature*, 360, 677–679.

Otake, S., Gowdy, P. D., & Cicerone, C. M. (2000). The spatial arrangement of L and M cones in the peripheral human retina. *Vision Research*, 40, 677–693.

Packer, O., Hendrickson, A. E., & Curcio, C. A. (1990). Development redistribution of photoreceptors across the *Macaca nemestrina* (pigtail macaque) retina. *Journal of Comparative Neurology*, 298, 472–493.

Packer, O., Williams, D. R., & Bensinger, D. G. (1996). Photopigment transmittance imaging of the primate photoreceptor mosaic. *Journal of Neuroscience*, 16, 2251–2260.

Pum, D., Ahnelt, P. K., & Grasl, M. (1990). Iso-orientation areas in the foveal cone mosaic. *Visual Neuroscience*, *5*, 511–523.

Rodieck, R. W. (1991). The density recovery profile: A method for the analysis of points in the plane applicable to retinal studies. *Visual Neuroscience*, *6*, 95–111.

Roorda, A., Metha, A. B., Lennie, P., & Williams, D. R. (1999). The packing arrangement of S, M and L cones in the living primate retina. *Investigative Ophthalmology and Visual Science Supplement*, *40*, 365.

Roorda, A., & Williams, D. R. (1999). The arrangement of the three cone classes in the living human eye. *Nature*, *397*, 520–522.

Rushton, W. A. H., & Baker, H. D. (1964). Red/green sensitivity in normal vision. *Vision Research*, *4*, 75–85.

Sekiguchi, N., Williams, D. R., & Brainard, D. H. (1993). Efficiency in detection of isoluminant and isochromatic interference fringes. *Journal of the Optical Society of America A*, *10*, 2118–2133.

Shapiro, M.B., Schein, S.J., & de Monasterio, F.M. (1985). Regularity and structure of the spatial pattern of the blue cones of Macaque retina, Journal of the American Statistical Association, pp. 803–814.

Williams, D.R. & Roorda, A. (2000). The trichromatic cone mosaic in the human eye. In: Gegenfurtner, K.R. & Sharpe, L.T. (Eds.), Color Vision: From Genes to Perception. Cambridge: Cambridge University Press, pp. 113–122.

Williams, D.R., Sekiguchi, N., Haake, W., Brainard, D., & Packer, O. (1991). The Cost of Trichomacy for Spatial Vision. In: Valberg, A. & Lee, B.B. (Eds.), From Pigments to Perception, New York: Plenum Press, pp. 11–21.